Simulation of an unsteady aeroelastic response of a multibladed rotor in forward flight

B. Cantaloube *, P. Beaumier **
ONERA
BP 72, 92322 Chatillon Cedex, France.

Abstract

This paper presents the implementation, in the ONERA ***elsA*** software, of a mesh deformation technique coupled with the ALE method for solving the Euler equations in the case of soft rotor blade applications. This method, taking advantage of the C or O topology of mesh blocks, has proven to be well adapted for such rotor applications. It uses, as input, the aeroelastic blade motion provided by a rotor trim analysis (HOST software of Eurocopter). Test cases concerning "Isolated Rotors in Forward Flight with Prescribed Deformations performed in the framework of the CHANCE program have been computed for inviscid flows and are presented for 7A and 7AD helicopter rotors for different flight conditions.

Introduction

The fluid-structure interaction problem is one of the major issue for prediction of aerodynamic rotor performances. Helicopter blades undergo strong deformations mainly due to aerodynamics loads and in the same time the resulting blade deformation has a non negligible influence on the aerodynamics of the rotor. The final goal of ONERA within the Franco-German CHANCE CFD Project is the strong coupling between fluid and structure response by means of coupling the structural dynamic Eurocopter's HOST software with the new object oriented aerodynamic ***elsA*** software [1]. This paper aims at describing and illustrating some mandatory tools developed in order to reach this objective.

The aerodynamic problem is tackled by means of the Arbitrary Lagrangian Eulerian method (ALE) for solving the unsteady Euler equations on deforming meshes.

An original technique, well adapted to rotorcraft applications, has been developed here. Each blade profile can undergo rigid body motion depending on flap, lag and torsional degrees of freedom given by a Fourier analysis provided by the structure code HOST [2] developed by EUROCOPTER.

Computations of unsteady inviscid flow around 7A and 7AD model rotors in forward flight have been performed for different flight conditions concerning some CHANCE test cases. Numerical results presented herein are compared with wind-tunnel test results in order to validate the "rigid blade and "soft blade functionalities.

Numerical methods

The Arbitrary Lagrangian Eulerian method (ALE) for soft rotor blades has been developed in the ONERA's ***elsA*** software and has already been tested in the case of the ONERA three-bladed 7A rotor with PF1 tip in forward flight with prescribed rigid blade motions [1].

Computing a flow past a deforming body such as a soft rotor blade needs to solve Euler or Navier-stokes governing equations on a moving grid.

In the finite volume formulation the governing flow equations solved on a moving grid are written under integral form :

$$\frac{d}{dt}\int_{\Omega}\mathbf{W}d\Omega+\oint_{\partial\Omega}Fc[\mathbf{W},\mathbf{s}].\mathbf{n}d\Sigma + \oint_{\partial\Omega}Fd[\mathbf{W},\mathbf{gradW}].\mathbf{n}d\Sigma=0 \quad (1)$$

in which the following notations have been used:

- The vector of conservative variables:

$$W=\begin{bmatrix}\rho\\ \rho\mathbf{U}\\ \rho E\end{bmatrix} \text{ with } \begin{cases}\rho=\text{density}\\ \mathbf{U}=\text{absolute velocity}\\ \rho E=\text{total energy}\end{cases}$$

- The convective fluxes:

$$\oint_{\partial\Omega}\boldsymbol{Fc}[\mathbf{W},\mathbf{s}].\boldsymbol{n}d\Sigma=\begin{bmatrix}\oint_{\partial\Omega}\rho(\mathbf{U}-\boldsymbol{s}).\mathbf{n}d\Sigma\\ \oint_{\partial\Omega}\rho\mathbf{U}\otimes(\mathbf{U}-\boldsymbol{s}+\boldsymbol{p}\mathbf{I}).\mathbf{n}d\Sigma\\ \oint_{\partial\Omega}[\rho\boldsymbol{E}(\mathbf{U}-\boldsymbol{s})+\boldsymbol{p}\mathbf{U}].\mathbf{n}d\Sigma\end{bmatrix} \quad (2)$$

---

* CFD and Aeroacoustics Department.
** Applied Aerodynamics Department.

- The diffusive fluxes:

$$\oint_{\partial\Omega} \mathrm{Fd}[\mathbf{W}, \mathbf{gradW}].\mathrm{nd}\Sigma = \begin{bmatrix} 0 \\ -\oint_{\partial\Omega} \tau.\mathbf{n}\mathrm{d}\Sigma \\ -\oint_{\partial\Omega} (\tau.\mathbf{U} - \mathbf{q}).\mathbf{n}\mathrm{d}\Sigma \end{bmatrix} \quad (3)$$

  τ is the viscous stress tensor
  and **q** is the heat transfer vector

- The grid velocity is noted **s** and $\frac{\mathrm{d}}{\mathrm{dt}}$ is a convective derivative. In equation (1), this derivative expresses that every elementary volume $\partial\Omega$ is convected with its velocity **s**.

The above equations show that only convective fluxes are affected by the grid velocity.

The following numerical applications concern only inviscid flows, then diffusive fluxes have been neglected.

Numerical scheme

The Euler equations are written in a rotating Cartesian coordinate system in which the conservation laws are expressed using the absolute velocity as unknown. They are discretized in space and time following the classical space-centered Jameson explicit scheme [3]. For the spatial discretization, a cell-centered finite volume formulation is used, which is of 2^{nd} order accuracy on smooth grids. For the time integration, a four step Runge-Kutta scheme is applied. The 2^{nd} and 4^{th} dissipation coefficients of the Jameson scheme have been respectively set to 1 and 0.064. Since the calculations concern an unsteady application, a constant time step is defined by the user in terms of azimuthal step $\Delta\Psi$. The addition of a simplified implicit stage [4] allows to increase the time step with respect to the stability limitation of the explicit scheme.

The Arbitrary Lagrangian-Eulerian deforming grid technique is used to account for the relative motion of the blades. The ALE formulation needs the knowledge of the mesh coordinates at every time in order to get the velocity of the mesh nodes by means of finite differences using a backward Euler scheme. Hence a new time dependent metric is computed. In the framework of the development of the ALE approach in *elsA*, we can choose first to compute the cell volume time variation by means of the well known GCL [5] conservation law which preserves the freestream conservation property. A second possibility is to use directly the cell dimensions (length, height, width) to compute the cell volume (lets call it the LHW technique). As it is mentioned in [1], the GCL formulation gives good results for a low increase in CPU time with respect to the LHW method.

The modifications of the numerical fluxes due to the ALE formulation are classical in Euler/Navier-Stokes codes. But the main issue raised by introducing such a technique in an industrial software as *elsA* is mainly to be able to tackle complex body deformations (here blade deformations) and hence make automatically and in any cases the mesh distort. In 'Arbitrary Eulerian Lagrangian', 'Arbitrary' means that the mesh can undergo any deformation provided that it fits the following boundary conditions:

- a given body deformation,
- outer boundaries are generally motionless (even if it is not mandatory).

Then, the mesh deformation can be computed by means of well known techniques. The most popular ones are the transfinite interpolation [6] and the spring analogy [7]. In the frame of this work, a well adapted technique, described below, has been developed.

Grid Deformation technique

The mesh deformation technique developed here, in the frame of rotor applications, is limited to structured meshes with C or O topology in the chordwise direction and H topology in the spanwise direction j allowing to define a finite number of blade profiles (j-profiles) which are the projection of a topological mesh plane (π(j)-plane noted π(p) on Figure 1) on the blade.

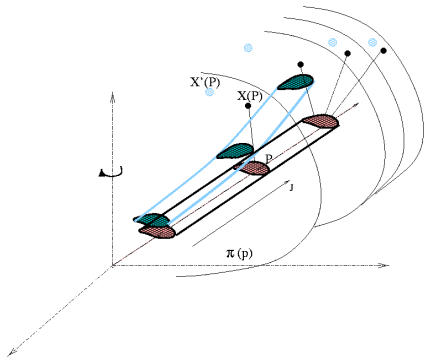

Figure 1: Blade surface deformation

Each j-profile (airfoil) undergoes only a rigid body motion (composed of translations and rotations) which induces the mesh deformation of the π(j)-plane. The last j-profile, at the blade tip, interferes on the j-planes ranging from the blade tip to the mesh outer boundary (Figure 1). For the sake of simplicity let us consider a unique j-profile interacting with a unique π(j)-plane (Figure 2).

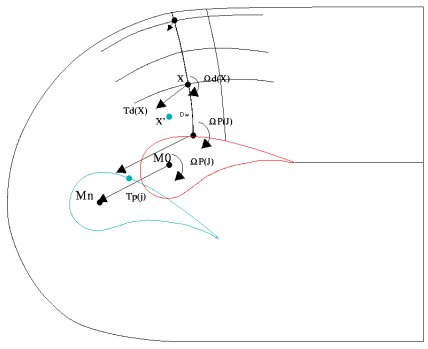

Figure 2: Profile deformation to mesh deformation

The profile motion results in a composition of translation $\mathbf{T_p}(j)$ and rotation $\mathbf{\Omega}_p(j)$ of which the unit orthogonal transformation matrix is $\mathbf{R_p}(j)$. As the boundary conditions impose the mesh to fit the profile contour and to be motionless on the outer boundaries, a damping function f(dw) and a damping transformation matrix $F(d_w)$ have been defined.

The dimensionless distance dw from any mesh point **X** to the profile is defined by:

$$dw = \frac{Dw}{Dw_{min}} \qquad (4)$$

where Dw is the distance from any mesh point **X** to the profile and Dw_{min} is the minimum size of the body adjacent cells in the direction orthogonal to the body.

Then mesh point displacements will result in a damped profile's translation **Td :**

$$\mathbf{Td}(\mathbf{X}) = \mathbf{Tp}(j)\, f(d_w) \qquad (5)$$

and in a damped rotation $\mathbf{\omega}_p(j)$ of which the matrix **Rd** is:

$$\mathbf{Rd}(\mathbf{X}) = \mathbf{Rp}(j)\, \mathbf{F}(d_w) \qquad (6)$$

The damping function f(dw) must decrease from 1 on the body boundary (dw = 0) to zero at infinity ($dw \to \infty$). Using an exponential function:

$$f(d_w) = Exp(-(\alpha d_w)^n) \qquad (7)$$

is an easy and straightforward way for meeting these boundary conditions. The higher the shape parameter n is the less is the size of the plateau of $f(d_w)$. The exponent n is generally chosen equal to 2. Then the size of the plateau is sufficient for tackling Navier-Stokes mesh deformation in the vicinity of the body. In this area, the mesh undergoes a quasi-solid body deformation and mesh overlapping cannot occur.

The parameter α is given by the equation:

$$\alpha = -\log(\varepsilon)/dw_{max} \qquad (8)$$

Which states that:

$$f(dw_{max}) \le \varepsilon \qquad (9)$$

In the following applications ε was arbitrarily chosen equal to 10^{-3} so that the displacement of the farthest node, lying on the outer boundary of the mesh block, can be neglected and taken equal to zero.

But overlapping can occur in the inner part of the mesh. Let's consider the following 1-D example of an extensible segment AB lying on the **x** axis of which A is the origin. The abscissa of A and B are respectively noted x_A and x_B with $x_B>0$. One of the extremity of segment, let's say A, undergoes a given translation T_A in the positive direction of the **x** axis and the other extremity has a free displacement smaller than a small positive quantity ε. Indeed one assumes that:

$$T_A < x(B) - x(A) \qquad (10)$$

The displacements of two close points C and D, between A and B, of which the respective abscissa are:

$$\begin{cases} x_C \\ x_D = x_C + dx; \ (dx > 0) \end{cases} \qquad (11)$$

are given by:

$$\begin{cases} T_C = T_A\, f(x_C) \\ T_D = T_A f(x_C + dx) \end{cases} \qquad (12)$$

Overlapping would occur, between A and B if:

$$x_C + T_A f(x_C) > x_C + dx + T_A(x_C + dx) \qquad (13)$$

From an asymptotic development it can be shown that overlapping can be prevented if:

$$-\frac{1}{T_A} < f'(x) < 0 \qquad (14)$$

Then, from the exponential definition of f(x):

$$f(x) = Exp(-\alpha x^n); \quad (\alpha > 0) \qquad (15)$$

and its derivative:

$$f'(x) = -\alpha m x^{n-1} Exp(-\alpha x^n) \qquad (16)$$

one readily obtains the following relation between α, x_m and n:

$$x_m = \frac{n-1}{\alpha^n} \qquad (17)$$

where x_m is an extremum for $f'(x)$.

Reporting (17) into (16) and then into (14) yields:

$$-\frac{1}{T_A} < -\alpha n x_m^{n-1} < 0 \qquad (18)$$

As f(x) decreases with respect to x and as the displacement of B must be smaller than a fixed positive value ε, x_m must be chosen such that:

$$x_A < x_m < x_B \qquad (19)$$

Finally, if n is chosen such as the exponential function (15), near the origin, is large enough (for example an uniform decrement in the vicinity of A) and x_m is chosen accordingly to equation (19), then equation (18) gives a range of values for α preventing overlapping. In 2-D the value of α, given by (8), should satisfy a constraint which would be similar to equation (18).

The damping matrix **F**(dw) is defined from f(dw) as:

$$\mathbf{F}(dw) = (\mathbf{I} - \mathbf{Rp}(j)^T)\, f(dw) + \mathbf{Rp}(j)^T \qquad (20)$$

where $\mathbf{R}^T$ means the terms of the transpose matrix of **R** and **I** is the unit matrix. Taking advantage that **Rp**(j) is a unit orthogonal matrix and replacing this equation in (6) yields the following expression for the rotation matrix **Rd**:

$$\mathbf{Rd}(\mathbf{X}) = \begin{cases} \mathbf{Rp} \text{ on the body } (dw = 0) \\ \mathbf{I} \text{ at infinity } (dw \to \infty) \end{cases}$$

From the above definitions of the damping function and the damping matrix (equations 7 and 20) the displacements of the vertex mesh have the following properties:

- on the body boundary the mesh undergoes the same translation and rotations as that of the body,
- the outer boundaries of the mesh are not influenced by the movement of the body.

In the case of "rigid blade computations", the blade motion is defined by the harmonic analysis of the rotation angles of the blade around the pitch, flap and lag hinges. For "soft blade computations", the blade deformations and rigid body motions are described by a modal approach. In this case, two output files from the HOST [2] code are required: a modal basis and the generalized coordinates. They give, for each j-profile, the translation vector **Tp**(j) and the rotation matrix **Rp**(j) taking into account the elastic deformation of the blade in flap, lag and torsion.

This deforming grid approach has been first used to manage the relative rigid blade motions for the unsteady inviscid flow around the ONERA three-bladed rotor with PF1 tip in forward flight [1]. For mono-block topology this technique is very close to that developed in the framework of the moving mesh strategy introduced initially in the ONERA code WAVES [8]. For multi-block topologies, the technique developed here depends only on the distance from a node to the body boundary and not on the mesh topology as it is the case in that developed in the WAVES code. Then, one can easily tackle deformation of multi-block defined meshes.

In order to give some idea of the behaviour of grid deformations involved around soft blades using the technique described above, we have considered the isolated 7A blade submitted to a deformation highly increased with respect to a real situation. Figure 3 and Figure 4 show partial views of the grids around the blade surface and around a blade section without (upper part) and with blade deformation (lower part).

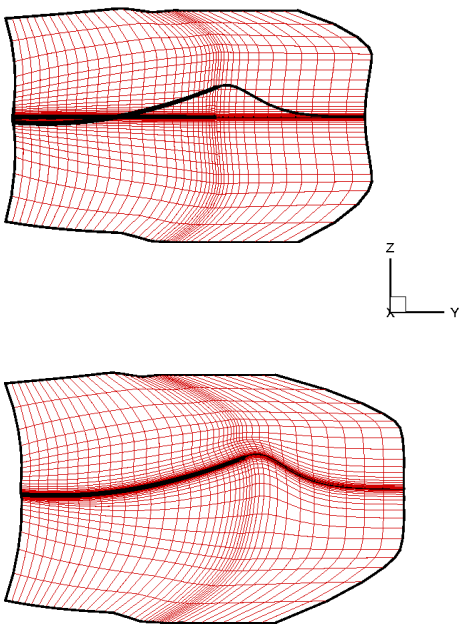

Figure 3: Partial views of grids around 7A blade: without (top) and with blade deformation (bottom)

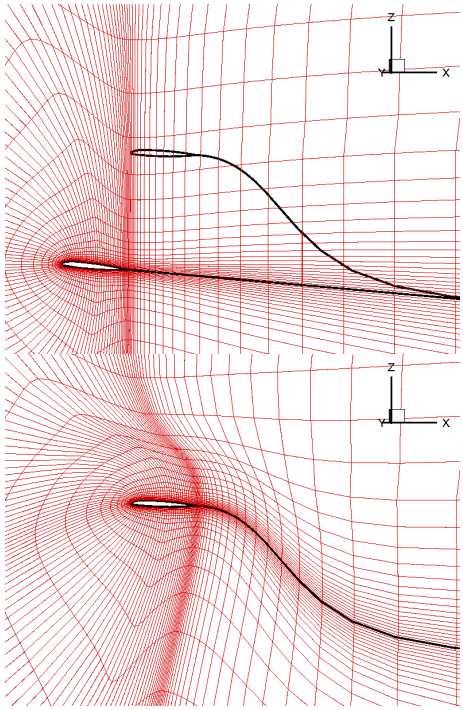

Figure 4: Partial views of grids around a 7A blade section: without (top) and with blade deformation (bottom)

Applications

ALE developments in ***elsA*** for soft blades have been done and results for the simulation of the unsteady inviscid flow around multibladed rotors in forward flight with prescribed blade deformation are presented below.

Boundary conditions

The following boundary conditions have been applied for all the applications:

- On the blade surface, a slip boundary condition is used (Euler calculations).
- For all far-field boundaries as well as for the most inboard boundary (near the hub), the boundary condition is a free stream condition. For these boundaries, the flow variables are treated following the concept of characteristic variables for non reflecting boundary conditions.
- Between the blocks, since the nodes are coincident, no extrapolation is used: such boundaries are equivalent to simple mesh cuts.

List of test cases

The test cases presented in this paper are those to be performed by ONERA for isolated rotors in forward flight in the frame of the CHANCE project.

Rotor	MODANE Test case	μ	CdS/Sσ	Zb= 200C_T/σ	$M_{\Omega R}$
7A	#312	0.4	0.1	12.56	0.646
7A	#317	0.4	0.1	14.80	0.646
7A	#321	0.4	0.1	17.47	0.646
7AD	#1224	0.4	0.1	12.51	0.646
7AD	#1228	0.4	0.1	15.06	0.646
7AD	#1232	0.4	0.1	17.53	0.646

Table 1: List of test cases

The test cases concern the 7A and 7AD rotors (Figure 5), tested in S1MA wind-tunnel during the 11th campaign [9]. These two rotors have four blades, equipped with OA213 and OA209 airfoils and only differ by the blade tip shape (from r/R=0.947 to r/R=1): the 7A blades are rectangular whereas the 7AD blades have a parabolic swept tip with anhedral. Both rotors have an aspect ratio AR=15 and a linear aerodynamic twist equal to -8.3°/R. During these tests, the rotors were trimmed according to the "Modane law (β_{1s}=0, β_{1c}= -θ_{1s}). The test cases selected for this study are defined by an advance ratio μ=0.4, a tip rotational Mach number $M_{\Omega R}$=0.646 and a fuselage drag coefficient CdS/Sσ=0.1. Several rotor lift coefficients Zb have been chosen, ranging from approximately 12.5 to 17.5 (Table 1).

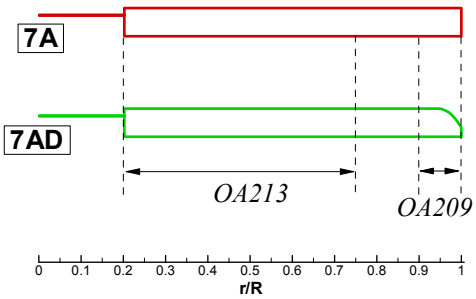

Figure 5: 7A and 7AD blades definition

Grids

The grids generated for this study are made of one C-H block per blade. For the 4-bladed, the grids have thus four blocks, each one including 141x40x26=146.640 nodes, with a total of 586.560 points. The grid extension is ±0.8R in the vertical direction (Z-axis) and 1.6R in the spanwise direction. The same grid topology was adopted previously when using the WAVES code [10].

A view of the grid for the 7AD rotor is plotted in Figure 6. This grid is not deformed. However, a collective pitch angle of 10° is introduced in the grid in order to limit the amount of deformation during the grid deformation process. To generate this grid, an analytical grid generator developed in [8] and similar to the one used in [11] has been used. A grid is generated around one blade; the grids around the other blades are deduced by rotations around the Z-axis, ensuring interfaces with coincident nodes between the blocks.

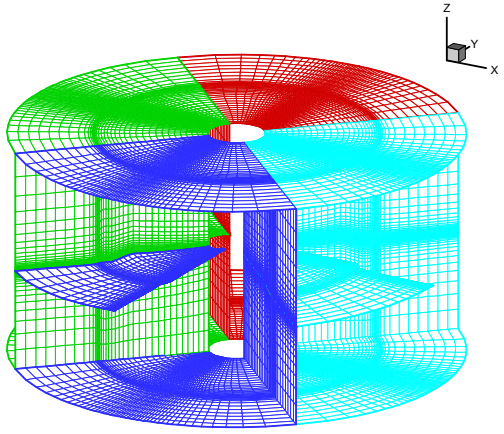

Figure 6: Non distorted grid around the 7AD rotor

Influence of blade deformations for the 7A rotor (test case #312)

The first computations are done with the *elsA* code for the 7A rotor, test case #312 (low lift: Zb=12.56). The time step chosen for this computation corresponds to Δψ=0.1°, so that one rotor revolution is described by 3600 time steps. The rigid and aeroelastic blade motion is obtained by HOST isolated rotor simulations.

The influence of the blade deformations on the sectional lift coefficients C_nM^2 time histories is illustrated on Figure 7 (HOST) and Figure 8 (*elsA*). It can be checked that the two codes predict the same tendencies. In particular, the amplitude and phase of the peak of negative airloads for the most outboard sections (r/R=0.975) are better predicted by the soft blade computations. This is due to the torsion elastic deformations which create negative incidences near the blade tip (Figure 9). Still, there are significant differences between the C_nM^2 coefficients predicted by *elsA* (soft blade) and experiment for r/R=0.975 on the advancing side, which are certainly a consequence of the lack of accuracy in the predictions of the torsion deformations (Figure 9).

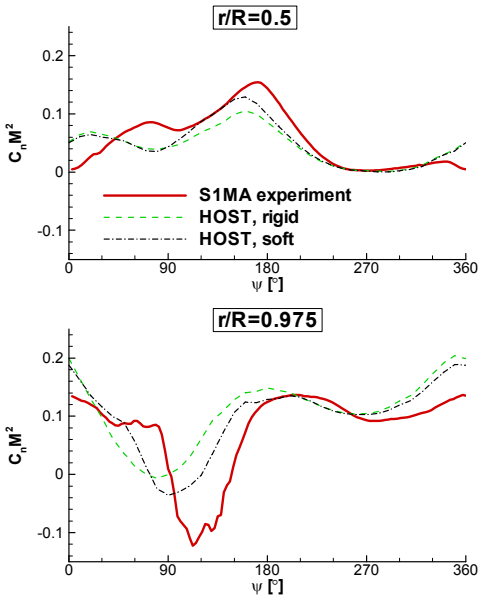

Figure 7: Influence of blade deformation on unsteady airloads (7A rotor, HOST vs. experiment)

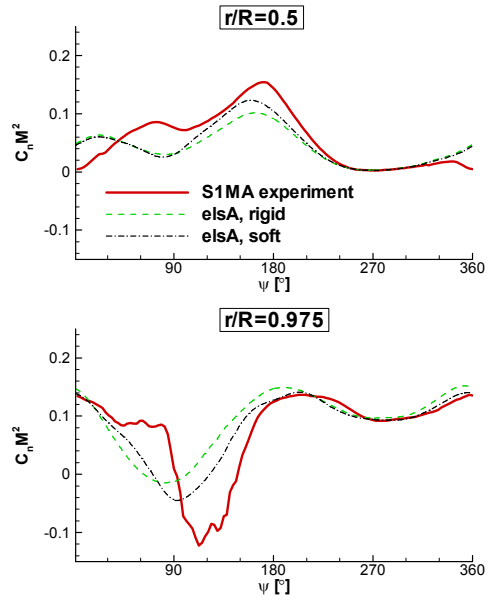

Figure 8: Influence of blade deformation on unsteady airloads (7A rotor, *elsA* vs. experiment)

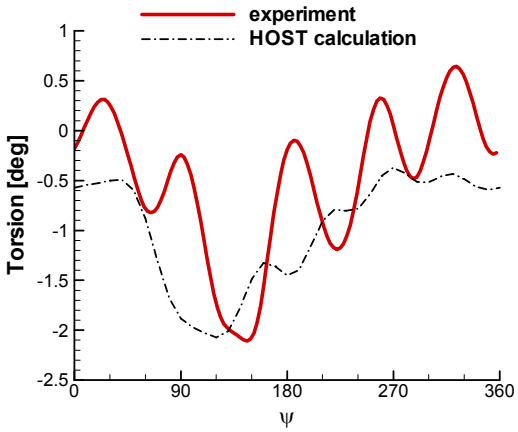

Figure 9: Torsion deformations at the tip of the 7A rotor

Figure 10 shows that the predicted rotor total thrust coefficient converges to a mean value close slightly lower than 12.5, which is the prescribed experiment value. It can be noticed that the amplitude of the oscillations of predicted thrust coefficient is larger in the soft blade calculation than in the rigid blade calculation. A similar trend is obtained in the HOST simulations. Note the quasi periodic evolution of the curve plotted in Figure 10 between ψ=180° and 360°, after a transient phase for 0°<ψ<180°. This shows that for such a high speed condition (μ=0.4), the solution becomes periodic after one rotor revolution.

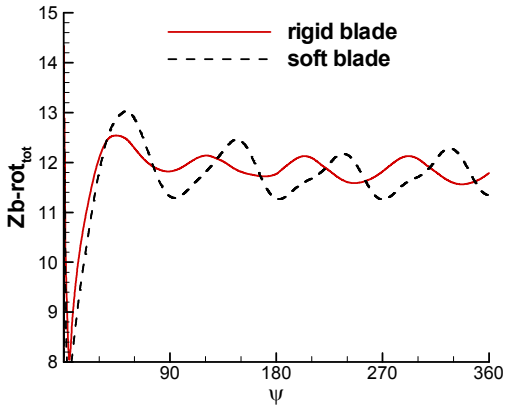

Figure 10: Influence of blade deformation on total rotor thrust history

The pressure distributions of the rigid and soft blade computations are compared to experiment in Figure 11. The agreement is fair in general. The largest influence of blade deformations is in the blade advancing side (ψ=120°) for the outer sections (r/R=0.975), where the shock positions are closer to the experiment in the soft blade computations, which is consistent with the airloads time histories of Figure 8. For the most inboard section (r/R=0.5), the agreement with experiment is not good on the retreating side (ψ=270°): in this part of the rotor disk, viscous effects play an important part and are not

included in the present Euler calculations.

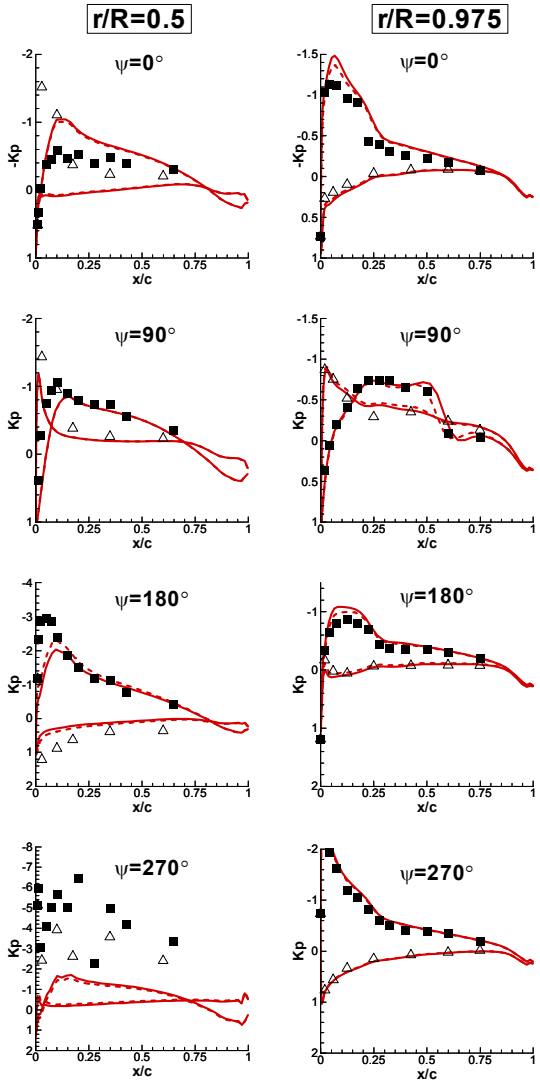

Figure 11: Influence of blade deformation on pressure distributions (7A rotor, *elsA* vs. Experiment)

7A/7AD comparison (low lift case)

The aerodynamic solution obtained for the 7A rotor on #312 test case (Zb=12.56) is compared with the solution for the 7AD rotor on #1224 test case (Zb=12.51). For stability reasons, the time step required to run the calculation of the 7AD rotor had to be reduced by a factor of 2 ($\Delta\psi$=0.05°) compared to the 7A rotor ($\Delta\psi$=0.1°). In both cases, the blade deformations come from simulations with the HOST code as it has been explained in the grid deformation paragraph.

On Figure 12 (upper part), the experiment shows that the shock waves location is located closer to the trailing-edge for the 7A rotor than for the 7AD rotor. Such a tendency is reproduced by the *elsA* calculations (lower part of Figure 12). It is reminded here that the 7AD blade tip (including sweep and anhedral) was designed at ONERA in order to reduce the shock waves intensity and to reduce the area of transonic flows appearing on the advancing side for high speed test conditions. The *elsA* calculation is able to capture this reduction of transonic flow for the 7AD blade compared to the 7A blade, as illustrated by Figure 13.

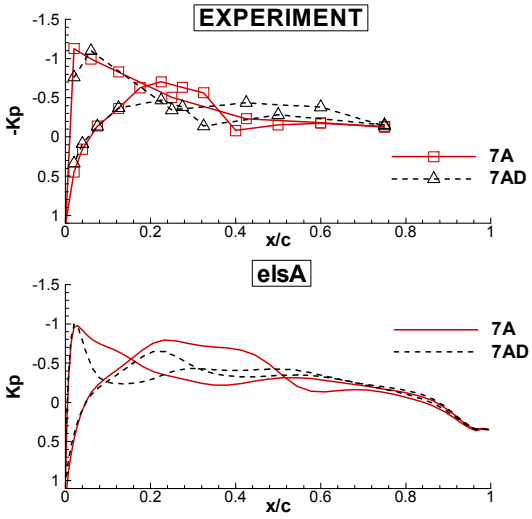

Figure 12: Pressure distributions on the 7A and 7AD blades (ψ=90°, r/R=0.975)

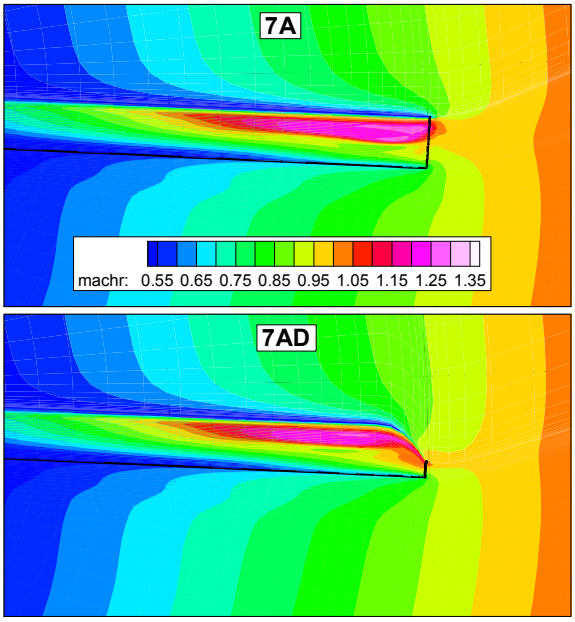

Figure 13: Influence of blade planform on relative Mach number contour levels (ψ=90°, μ=0.4)

Influence of rotor lift

In this paragraph, the same grid (the one generated for the lowest value of Zb) is used for the all computations of the 7A rotor.

Contour plots of lift coefficients C_nM^2 show that the increase of Zb generates more lift in the front and rear

parts of the rotor disk; this is true for the two rotors, 7A (Figure 14) and 7AD (Figure 15). This trend is well predicted by the calculations. Figure 14 and Figure 15 also show the systematic phase lag of the area of minimum (negative) lift in the calculation compared to experiment.

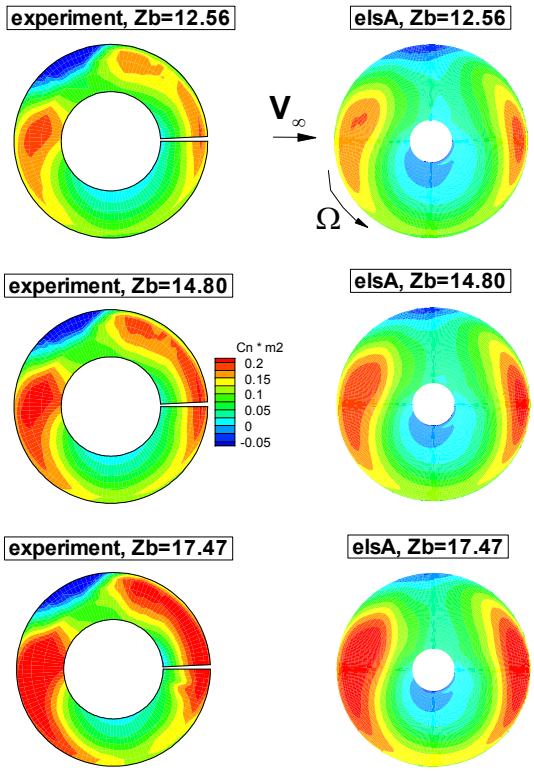

Figure 14: Influence of rotor lift coefficient on airloads distributions (7A rotor)

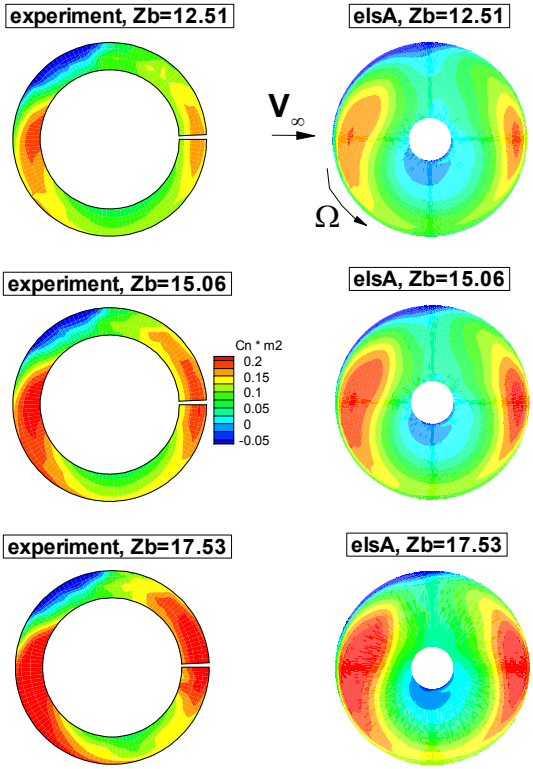

Figure 15: Influence of rotor lift coefficient on airloads distributions (7AD rotor)

Conclusion

The deforming grid approach ALE, first developed for rigid blade applications has been extended, in the frame of this work, for soft blade applications and has been coupled with a mesh deformation technique which has proven to be well adapted for rotor applications. As shown in this paper, this technique can tackle large amplitude deformation of soft blades. This technique needs as an input the information of the rigid and aeroelastic rotor blades motion (provided by the HOST code for the present applications). In the vicinity of the blade, the mesh undergoes a quasi-solid deformation. This property confers to this technique to be readily applicable to Navier-Stokes mesh deformations preventing for mesh overlapping phenomenon in this area.

The test cases concerning “Isolated Rotors in Forward Flight with Prescribed Deformations performed in the framework of the CHANCE program have been successfully computed. The results obtained are in fair agreement with experimental results.

In a near future, the ALE technique will be combined with the CHIMERA grid technique already developed at ONERA [12]. Such a method will be mandatory in order to compute a full helicopter including main rotor, tail rotor and fuselage.

Acknowledgements

This work was conducted as part of the French/German cooperative research program CHANCE. The authors would like to acknowledge the French Department of Defence DGA/SPAe as well as the French Agency for Civil Aviation DGAC for their financial support.

References

[1] J.C. Boniface, B. Cantaloube, A. Jolles *"Rotorcraft simulations using an Object Oriented approach."* . 26th ERF . The Hague (The Netherlands), Sept 26-29,2000.

[2] B. Benoit, A.M. Dequin, K. Kampa, W. von Grunhagen, P-M. Basset, B. Gimonet. *"HOST, a General Helicopter Simulation Tool for France and Germany"*. 56th AHS Forum, Virginia Beach (USA), May 02-04,2000.

[3] A. Jameson, W. Schmidt, E. Turkel. *"Numerical Solution of the Euler Equations by Finite Volume Methods using Runge-Kutta Time Stepping Schemes"*. AIAA Paper 81-1259,1981.

[4] A. Lerat, J. Sides, V. Daru, *"An Implicit Finite-Volume Method for Solving the Euler Equations"*. Lecture Notes in Physics, Vol. 170, Springer-Verlag, 1982.

[5] P.D. Thomas and C.K. Lombard. *"Geometric Conservation Law and its Application to Flow Computations on Moving Grids"*. AIAA Paper 78-1208,1978.

[6] J. T. Batina. *"Unsteady Euler airfoil solutions using unstructured dynamic meshes"*. AIAA journal, No 8, August 1990.

[7] A.L. Gaitonde, S. P.Fiddes. *"A three dimensional moving mesh method for the calculation of transonic flows"*. Aeronautical Journal of the Royal Aeronautical Society, May 1995.

[8] J. C. Boniface, B. Mialon, J. Sides. *"Numerical Simulation of Unsteady Euler Flow Around Multibladed Rotor in Forward Flight using a Moving Grid Approach"*. 51st AHS Forum, Fort Worth, Tx. (USA), May 1995.

[9] J.P. Drevet, "*11eme campagne de rotors d'helicopteres dans la soufflerie S1MA. Rotors 7A et 7AD1. Deuxieme partie"*. Mai 1991, PV 5/8467 GY, Fevrier 1992

[10] G. Reboul, "*Modification d'un code Euler pour la prise en compte de la souplesse des pales dans le calcul de l'ecoulement autour d'un rotor d'helicoptere* . Rapport de stage ONERA Sup'Aero, juin 1998

[11] P. Beaumier, E. Chelli, K. Pahlke *"Navier-Stokes prediction of helicopter rotor performances in hover including aero-elastic effects"*. 56th AHS Forum, Virginia Beach (USA), May 02-04,2000.

[12] C. Benoit, G. Jeanfaivre, *"3D Inviscid Isolated Rotor and Fuselage Calculations Using Chimera and Automatic Cartesian Partitioning Methods"*. AHS Aeromechanics Specialists Meeting, Atlanta, Georgia (USA), November 2000.